

Fine Scale alpha Precipitation in Ti-19at.%V in the Absence of Influence from omega Precipitates

A. Sharma¹, V. Soni¹, S. Dasari¹, S.A. Mantri¹, Y. Zheng^{2#}, H. Fraser^{2*}, and R. Banerjee^{1*}

¹ Department of Materials Science and Engineering, University of North Texas, Denton, TX, 76191, USA

² Department of Materials Science and Engineering, The Ohio State University, Columbus, OH 43210, USA

Presently at Department of Chemical and Materials Engineering, University of Nevada Reno, Reno, NV, 89557, USA

* Corresponding author: fraser.3@osu.edu, Raj.Banerjee@unt.edu

Abstract

While the isothermal omega-assisted mechanism of homogeneously distributed fine scale alpha precipitation has been well-documented in several titanium alloys, including Ti-19at%V (Ti-20wt%V), this paper reports that a similar type of alpha precipitation may occur in the absence of any direct or indirect influence of omega precipitates. Rapid heating of a beta solution-treated and quenched Ti-19at.%V alloy to 500°C results in destabilization of the congruent athermal omega precipitates, followed by the development of compositional fluctuations in the form of Ti-rich or V-depleted pockets during isothermal holding, as revealed by atom probe tomography. These pockets possibly result from beta phase separation and may subsequently act as homogeneously distributed alpha nucleation sites.

Keywords: *β-Titanium alloy, α distribution, APT, phase separation, Miscibility gap*

Titanium-base alloys comprise an important class of high strength lightweight structural alloys, suited for both ambient as well as intermediate temperature applications [1,2]. Amongst the different classes of titanium alloys, β Ti alloys, specifically metastable β alloys, offer the ability to tune the microstructure and resulting mechanical properties over a wide range. Such variations can be introduced via carefully designed thermo-mechanical processing pathways [3]. β Ti alloys

are often used as components in their $\alpha+\beta$ processed condition, typically comprising of relatively coarse equiaxed α precipitates in the β matrix.

In contrast, some recent reports focus on obtaining an homogenous microstructure with a fine scale distribution of intra-granular α precipitates, via non-conventional transformation pathways [4–8]. Thus, several reports discuss using isothermal ω precipitates as potential α nucleation sites, in metastable β -Ti alloy. These precipitates act as potent α nucleation sites due to three factors; firstly, they are β solute depleted regions with a higher local chemical potential based driving force; secondly, the local stress fields arising from the β/ω misfit adds to the driving force; and thirdly, the β/ω interface acts as a heterogeneous nucleation site [9–13]. Additionally, entrapment of oxygen at these interfaces has also been proposed to promote α nucleation, oxygen being a strong α stabilizer [6,8,13]. Since these isothermal ω precipitates are present uniformly throughout the β matrix, the resultant microstructure from these non-conventional routes, is a fine distribution of α precipitates within the β matrix, resulting in impressive mechanical properties [10,14–17]. On similar lines, in systems with high β/ω misfit, it has been observed that structural defects at the β/ω interface, such as terraces and ledges actively promote α nucleation, leading to a refined microstructure [5–8,11]. The concentration field and the stress field of the ω precipitates along with their degree of coherency and precipitate size are some of the factors influencing this mechanism also referred to as the direct impact of ω precipitates on α nucleation [12].

An alternative, indirect, role that isothermal ω precipitates may play regarding α nucleation within the β grains, was reported by Zheng et al. [18,19], in case of the β alloy Ti-5Al-5V-5Mo-3Cr (also referred to as Ti-5553). This mechanism involves the initial development of isothermal ω precipitates, involving rejection of β stabilizing alloying elements, during the slow heating of a solution treated and quenched sample. Continued heating above the ω solvus temperature results in dissolution of the isothermal ω precipitates but retains the solute lean pockets within the β matrix. Such solute lean pockets subsequently act as the nucleation sites for α precipitates due to their favorable chemical potential (driving force), resulting in a refined and homogeneous α distribution [19].

While the prior two proposed mechanisms involved influence of isothermal ω precipitates on fine scale α precipitation, Nag et al. [20,21] observed that a refined α -distribution could be obtained even with a single-step heat treatment in the absence of any influence from ω precipitates. This is achieved by the “pseudospinodal” mechanism, where local compositional fluctuations within β grains result in nucleation of α with non-equilibrium compositions which then grow with time while approaching their respective equilibrium compositions, similar to spinodal decomposition. However, the applicability of this route to engineer fine-scale microstructures remains limited as Boyne et al. observed based on phase-field studies that this mechanism can be activated only for a narrow range of alloy compositions in the vicinity of the temperature dependent $C_0(T)$ point, where the free energies of α and β phases become equal [22].

As mentioned earlier, for high β/ω misfit systems, such as Ti-19at.%V, the development of ω -assisted fine scale α distribution has been well-documented and rationalized [11,12]. However, the possibility of obtaining a fine scale α distribution *in the absence* of any direct or indirect influence

from ω precipitates, has not yet been explored. Therefore, in this study we compare intra-granular α nucleation in Ti-19at%V with and without any direct influence from ω precipitates. To achieve this, we compare the α distribution from three different heat treatments, detailed below.

An ingot with the nominal composition of Ti-19at.%V (Ti-20wt.%V) was vacuum arc melted over a water-cooled copper hearth. This ingot was homogenized under vacuum at 1000°C for 7 days and then β -solutionized at 900°C for 30 minutes, followed by water quenching to room temperature. Smaller pieces were cut out from this β -solutionized ingot which were then subjected to three different heat-treatments. The first heat-treatment [11,12] (hereby known as *Two-step aging*) consisted of aging the sample at 375°C for 50 hours and then water quenching to room temperature. This was followed by a second aging step which consisted of heating at 500°C for 20 hours, again followed by water-quenching. For the second heat-treatment (referred to as *Single-Step aging, 500°C*), samples were directly aged at 500°C for 20 hours (with some samples aged at intermediate time-steps of 30 mins, 1 hour and 10 hours) and then water-quenched. The third heat-treatment was similar to the second, but aging was undertaken at 600°C for 20 hours, hence termed *Single-Step aging, 600°C*. Microstructural characterization of these samples was carried out using scanning electron microscopy (SEM) using an FEI Nova NanoSEM. Microstructural quantification was carried out using MIPAR software [23]. TEM foils were prepared from the samples using the FEI Nova 200 NanoLab FIB/SEM and these foils were imaged in a FEI make Tecnai G2 F20 S/TEM. For local compositional analysis, 3D atom probe tomography (APT) was carried out for these samples in a CAMECA LEAP 3000 HR instrument. All the APT characterization was carried out in voltage evaporation mode (at a rate of 0.5%) at a temperature range of 40-60 K. The pulsing voltage was held at 20% of the steady state voltage at a frequency of 200kHz. Data was analyzed using Cameca's IVAS software (version 3.6.8).

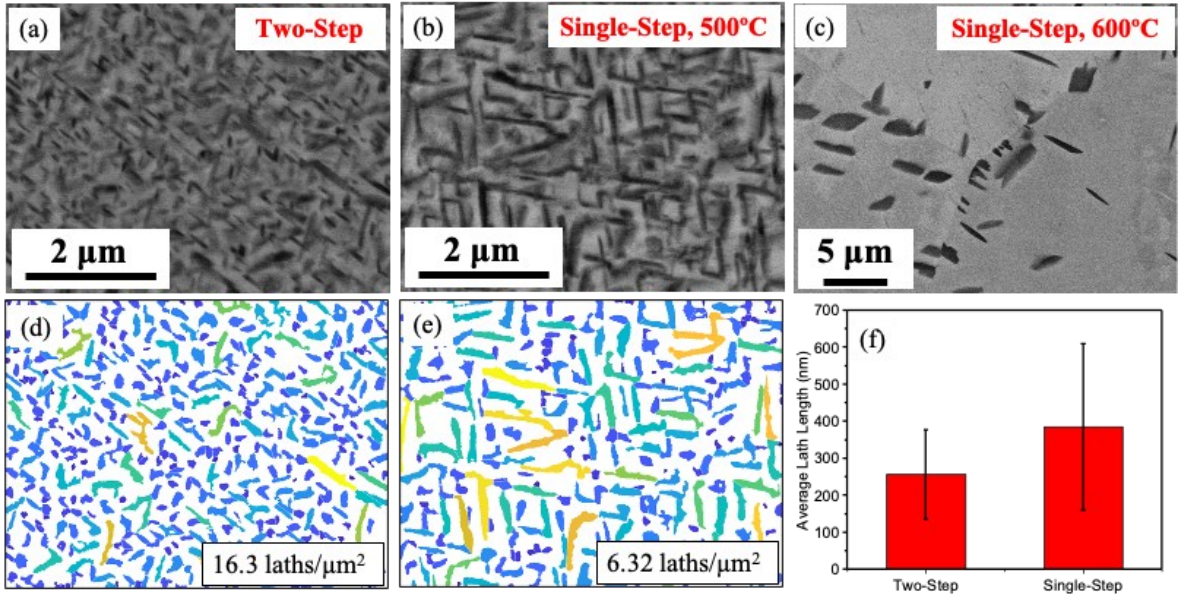


Figure 1. SEM micrographs (BSE contrast) from (a) Two step heat treatment (b) Single step heat treatment. (c) No intra-granular α nucleation seen after aging at 600°C. (d) and (e) are the respective processed images highlighting α laths along with the respective areal number densities (colors randomly assigned to identify individual laths). (f) The α distribution is slightly coarser after single-step aging.

The microstructures from the three different annealing treatments have been compared in Figure 1. Figures 1(a) and 1(b) show backscatter SEM images from the first two annealing treatments. Figure 1(a) shows a fine scale α distribution after the two-step annealing ($375^{\circ}\text{C}/50$ hrs + $500^{\circ}\text{C}/20$ hours). Such a refined distribution of α laths is a consequence of ω -assisted α precipitation, as reported previously by Zheng et al. [11] and Shi et al. [12]. Interestingly, a relatively fine scale α distribution is also observed, after the single step annealing ($500^{\circ}\text{C}/20$ hours) albeit it is not as refined as that for the two-step case. The α laths have nucleated homogenously within the β grains without any significant heterogenous grain boundary α precipitation. The α distribution from the two-step and single-step annealing conditions have been compared and quantified using image analysis tools within the MIPAR platform [23]. The segmented images are shown in Figures 1(d) and (e), corresponding to the SEM images shown in Figures 1(a) and (b) respectively. The estimated number density of α laths for the two-step annealing is 16.3 laths/ μm^2 , while it is 6.32 laths/ μm^2 after single-step annealing. A tighter distribution of α -lath lengths is evident after the two-step treatment, as compared with the single-step treatment, as shown in Figure 1(f). Figure 1(c) shows a backscatter SEM image from the third heat-treatment, involving single-step annealing at 600°C . Interestingly, there is no significant intra-granular fine scale α precipitation in this case, but rather coarse α precipitates, predominantly in the vicinity of grain boundaries, is observed.

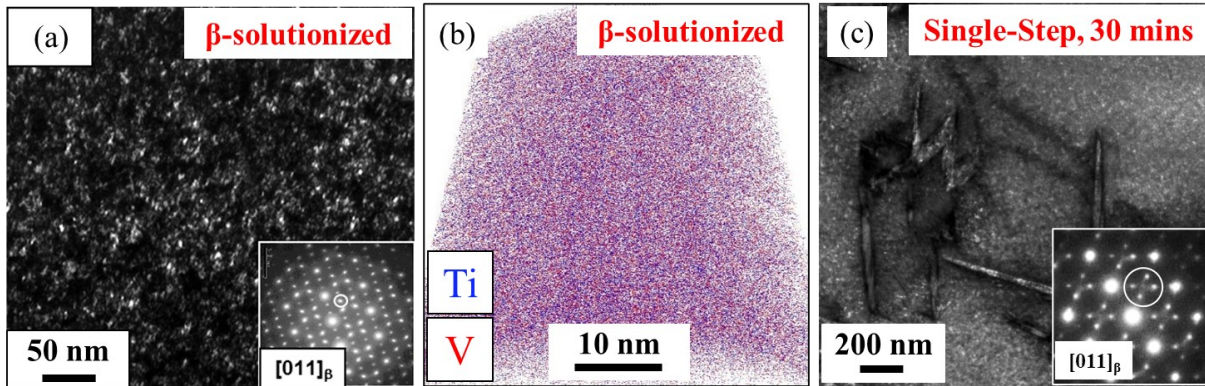


Figure 2. Microstructure at early stages of single-step aging at 500°C (a) DF-TEM from β -solutionised sample showing presence of athermal ω (b) APT ion-map reconstruction showing no significant compositional partitioning at this stage. (c) DF-TEM image showing presence of α laths along with athermal ω precipitates. Corresponding TEM diffraction pattern in the inset reveals the presence of both α and ω phases

Further investigation of the mechanism of α nucleation during single-step annealing has been carried out via single-step isothermal annealing at 500°C for progressively increasing time periods. Prior to annealing, after quenching from the β phase-field, the microstructure consists of a fine distribution of athermal ω precipitates as visible in the dark-field (DF) TEM image shown in Figure 2(a). At this stage, no compositional partitioning between the ω and β phases was observed, as shown in the atom probe reconstruction in Figure 2(b). This confirms the congruent nature of these athermal ω precipitates, in agreement with previous reports [24]. After 30 minutes annealing at 500°C , fine α -laths start to nucleate within the β grains as shown in the dark-field TEM image in Figure 2(c) and the corresponding diffraction pattern in the inset. Additionally, fine scale athermal ω precipitates are visible in the untransformed regions of the β matrix, which form during the

quench from 500°C to room temperature. Distinct compositional partitioning between the α and β phases is observed at this stage, shown in the APT results in Figures 3(a) and (b). The α precipitates have a composition 97.35at.%Ti – 2.65at.%V, while the adjacent β matrix has a composition 74.3at.%Ti – 25.7at.%V. In regions away from α laths, extremely small-scale compositional fluctuations could be detected in the APT results. Figures 3(e) shows the Ti and V ion map for this sample. At this scale, both types of the fluctuations appear to be distributed homogenously. A 30nm \times 30nm \times 40nm volume was extracted from this reconstruction (marked by the dashed square in Figure 3(e)), and this was subjected to cluster analysis routines in IVAS software [25,26]. The cluster analysis revealed Ti-rich (Figure 3(f)) regions within the volume, with an average composition of Ti-7.9at.%V, see the table in Figure 3(g). These compositional fluctuations may correspond to the onset of phase separation within the β phase, consistent with the miscibility gap experimentally reported in the Ti-V binary system [27–32]. Therefore, at early stages of the precursory β phase separation, during aging at 500°C, a large number of small-scale compositional fluctuations arise within the β matrix. However, all these fluctuations are not of the same amplitude. The reported sigma value of 2% in Fig. 3(g) corresponds to a variance of 4% ($s = \sigma^2$) which means that the composition of Ti-enriched (V-depleted) pockets vary from \sim 86.5 at.% Ti to \sim 96.5 at.% Ti. With increasing aging time, the large number of small-scale fluctuations develop into a small number of larger-scale pockets, which are substantially enriched in Ti, and eventually act as α nucleation sites.

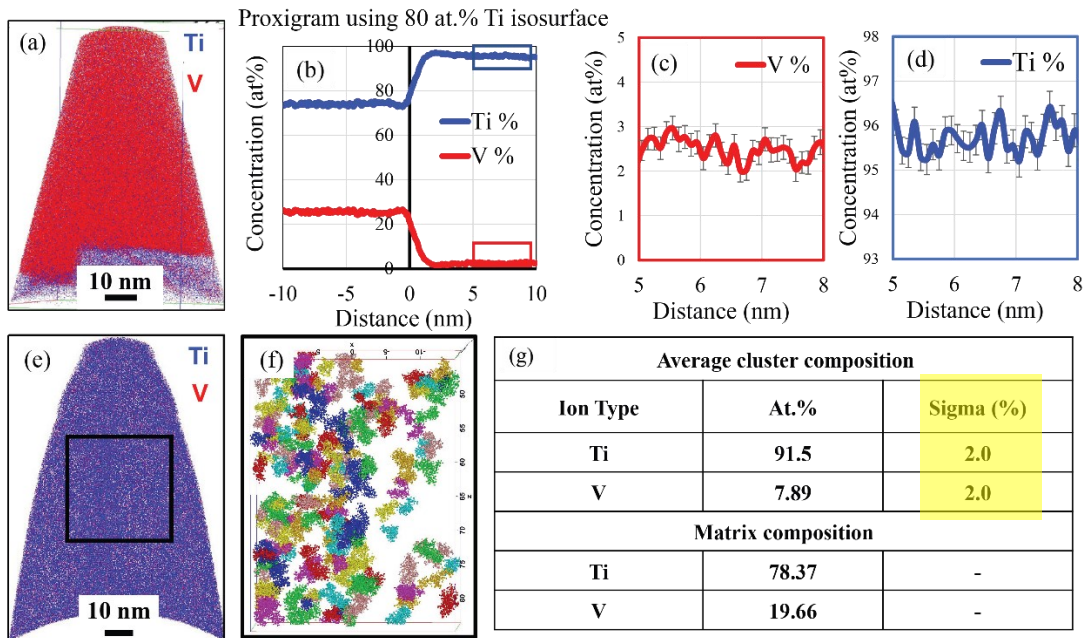


Figure 3. Compositional partitioning after 30 minutes of single-step aging at 500°C (a) APT reconstruction with superimposed Ti and V ions maps from an α lath with the corresponding proxigram shown in (b). The regions enclosed in red and blue rectangles are blown up in (c) and (d) respectively, for clarity. (e) Ion-map of a region away from an α lath. The volume enclosed in dotted square was extracted for cluster analysis. (f) shows the presence of Ti clusters, in the extracted region which develop at early stages of single-step heat treatment due to phase separation. The clusters have been assigned different colors randomly to identify them distinctly. (g) Average cluster and matrix composition from APT.

The evolution of α precipitate density, and the area fraction of the α phase, as a function of annealing time, has also been investigated. The results are shown in Figure 4, showing that both these quantities increase with isothermal annealing time at 500°C, indicating that the nucleation of new α precipitates continues during aging. Additionally, the change in average length of α lath was also evaluated as a function of aging time (Figure 4(f)). The average size of these α laths/plates for aging times of 1 hr, 10 hrs, and 20 hrs at 500°C, are 467 ± 257 nm, 576 ± 299 nm, and 472 ± 268 nm respectively. Therefore, there is no statistically significant difference in the size of these α laths/plates with increasing aging time.

The refined nucleation of the α phase within the β grains, during the single step annealing at temperatures above ω solvus has been previously observed in the case of Ti-5553 [20]. This was ascribed to a pseudo-spinodal decomposition pathway resulting from the local chemical fluctuations. Although similar nano-scale compositional fluctuations are observed in the APT results from the 500°C/30 mins annealed sample (Figure 3) of the Ti-19at.%V alloy in the present study, pseudo-spinodal is an unlikely decomposition mechanism in the present case. This is because the nominal composition of the present alloy is far from the $C_0(T)$ composition (intersection of α and β free energies at 500°C) modeled using solution thermodynamics based CALPHAD approaches (PANDAT) as shown in [Supplementary Figure S1](#), whereas previous studies clearly establish that the pseudo-spinodal mechanism can only be activated if the nominal

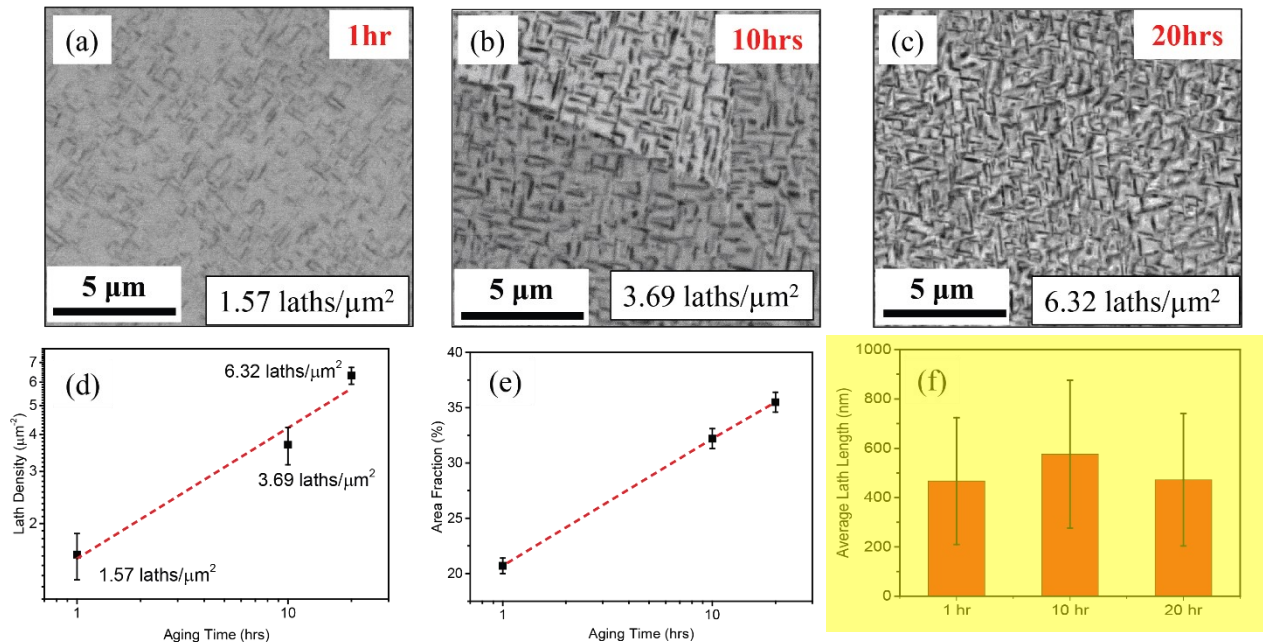


Figure 4. During the single-step heat treatment at 500°C, intra-granular α phase nucleates as shown by SEM micrographs (BSE contrast) after holding for (a) 1 hour, (b) 10 hours and (c) 20 hours. Note complete absence of coarser heterogenous α laths typically found at grain boundaries. Variation with aging time in (d) Area fraction of α phase, (e) Average α lath density, and (f) Average α lath length.

alloy composition lies close to $C_0(T)$ [20,22]. This could also be attributed to presence of inaccuracies within the Ti database used in PANDAT computations. Interestingly, in the present case, although the experimentally observed phase fraction of α phase for Ti-19at.%V is in good

agreement with the PANDAT predictions, the computed version of Ti-V binary phase diagram does not exhibit the β miscibility gap which has been reported in previous experimental studies [27–29,33]. The possibility of pseudo-spinodal mechanism is further ruled out based on the compositions of α and β phases after 30 minutes of aging, α : 97.4at%Ti–2.6at%V and β : 65.1at%Ti–34.9at%V. While the α composition is close to the predicted equilibrium composition from PANDAT, α : 99.2at%Ti–0.8at%V, pseudospinodal decomposition would warrant this composition to be far-from equilibrium [4]. The composition of β : 65.1at%Ti–34.9at%V is far-from the equilibrium composition predicted by PANDAT (β : 74.3at%Ti–25.7at%V) since the thermodynamic database used for these predictions (PanTi database) does not account for the β miscibility gap.

Another mechanism ruled out in the present case is one where α nucleates due to the indirect effect of the ω phase [18]. This is not likely in the present case since this mechanism can only operate after a significant period of annealing below the ω -solvus (in the temperature range of 350–375°C). This allows sufficient time for compositional partitioning between the ω and the β phases via diffusion, leading to the formation of isothermal ω precipitates. In the present case, the quenched alloy solely contains congruent athermal ω precipitates (Figure 2(a)) which are compositionally identical to the parent β matrix (Figure 2(b)). Direct annealing at 500°C (a temperature higher than the ω -solvus) does not offer sufficient time for these athermal ω precipitates to reject V by diffusion, and therefore the V-depleted compositional pockets observed in the APT results, cannot form via this mechanism.

When the beta-solutionized and quenched sample is heated to 500°C, the athermal ω precipitates are de-stabilized and transform back into the parent β phase via a displacive (diffusionless) process. At 500°C, the Ti-19at.%V composition lies within the miscibility gap within the beta phase. Therefore, longer term annealing at 500°C results in a phase separation within the beta matrix, resulting in the formation of nanometer scale Ti-rich pockets. These Ti-rich pockets were detected via atom probe tomography (APT) as shown in Figures 3(e), (f), and (g). Evidence for such phase separation within the beta matrix of Ti-V alloys has also been previously discussed in the literature [30–32]. These Ti-rich pockets have a range of compositions, and those pockets which have a composition close to the equilibrium composition of the α phase at 500°C, act as nucleation sites for α laths [12]. This is confirmed by comparing the compositions of these α laths experimentally estimated from APT (Ti:97.4 at%, V:2.6 at%) and those predicted by PANDAT (Ti:99.2 at%, V:0.8 at%), which are very close to each other. ***The observation of such compositional pockets is only possible due to a phase separation within the β matrix prior to α nucleation.*** While classical intragranular nucleation is also based on composition fluctuations leading to α nucleation, it is not possible to experimentally capture these fluctuations in a sample quenched to room temperature. This is due to the fact that these fluctuations are highly transient in nature, lead to an increase in the free energy of the local β pocket, and will only be stabilized after they transform to α precipitates. In contrast, the fact that these compositional pockets/fluctuations are present in the quenched beta matrix, prior to forming α precipitates, is strongly indicative of a phase separation within the β matrix.

This can also explain the lack of refined intra-granular α precipitates at 600°C, since the β miscibility gap for Ti-19at.%V presumably lies between 500°C and 600°C [27–31,33]. At 600°C, the alloy is no longer within the β miscibility gap and therefore there is no β phase separation prior to α nucleation. Based on phase-field modeling coupled with computational thermodynamics, Zhang et al. have recently reported a novel route to engineer heterogenous microstructures in the Ti-V binary system, which also exploits the presence of the β miscibility gap in this system [33].

The present study clearly reveals the formation of a refined homogeneous intra-granular distribution of α precipitates within the β matrix of a Ti-19at.%V alloy by direct single-step annealing at 500°C. This temperature is substantially greater than the ω -solvus temperature and therefore the α phase nucleates without any direct or indirect influence from ω precipitates. The distribution is somewhat less refined as compared with that from the two-step ω -assisted α nucleation mechanism. APT results indicate that during the early stages of annealing at this temperature, Ti-rich (V-depleted) clusters or pockets are formed which act as potent nucleation sites for the α precipitates. These extremely fine clusters or pockets possibly originate from the phase separation within the β matrix, due to the reported miscibility gap present in this Ti-V binary system [27–30,32,33]. However, further investigations are required to conclusively establish the presence of such a miscibility gap. When aged at a marginally higher temperature of 600°C, only coarse α laths are observed, primarily nucleating heterogeneously in the vicinity of grain boundaries, which is in contrast to the fine scale microstructure obtained after annealing at 500°C. These observations indicate that the miscibility gap for this composition lies between 500°C to 600°C and therefore at temperatures such as 600°C, β phase separation is absent. The prospect of the pseudo-spinodal mechanism of α precipitation, previously observed for other alloy systems, has been eliminated in the present case based on CALPHAD calculations, as well as by measuring the early-stage compositions of both α and β phases. Based on the experimental observations, the proposed transformation pathway for α precipitation observed in the present study is: β phase-separates into $\beta 1$ (Ti-rich pockets) and $\beta 2$ (Ti-lean pockets) where α nucleates along $\beta 1$.

Acknowledgments: This research has been supported by the National Science Foundation (NSF), Division of Materials Research (DMR) under grants DMR-1905844 and DMR-1905835.

References:

- [1] C. Leyens, M. Peters, Titanium and Titanium Alloys: Fundamentals and Applications, John Wiley & Sons, 2003.
- [2] D. Banerjee, J.C. Williams, *Acta Materialia* 61 (2013) 844–879.
- [3] Titanium, Springer Berlin Heidelberg, Berlin, Heidelberg, 2007.
- [4] S. Nag, R. Banerjee, R. Srinivasan, J.Y. Hwang, M. Harper, H.L. Fraser, *Acta Materialia* 57 (2009) 2136–2147.
- [5] F. Prima, P. Vermaut, G. Texier, D. Ansel, T. Gloriant, *Scripta Materialia* 54 (2006) 645–648.

[6] T. Li, D. Kent, G. Sha, M.S. Dargusch, J.M. Cairney, *Scripta Materialia* 104 (2015) 75–78.

[7] Y. Ohmori, T. Ogo, K. Nakai, S. Kobayashi, *Materials Science and Engineering: A* 312 (2001) 182–188.

[8] T. Li, D. Kent, G. Sha, L.T. Stephenson, A.V. Ceguerra, S.P. Ringer, M.S. Dargusch, J.M. Cairney, *Acta Materialia* 106 (2016) 353–366.

[9] B. Song, Y. Chen, W. Xiao, L. Zhou, C. Ma, *Materials Science and Engineering: A* 793 (2020) 139886.

[10] O.M. Ivasishin, P.E. Markovsky, S.L. Semiatin, C.H. Ward, *Materials Science and Engineering: A* 405 (2005) 296–305.

[11] Y. Zheng, D. Choudhuri, T. Alam, R.E.A. Williams, R. Banerjee, H.L. Fraser, *Scripta Materialia* 123 (2016) 81–85.

[12] R. Shi, Y. Zheng, R. Banerjee, H.L. Fraser, Y. Wang, *Scripta Materialia* 171 (2019) 62–66.

[13] J. Coakley, A. Radecka, D. Dye, P.A.J. Bagot, H.J. Stone, D.N. Seidman, D. Isheim, *Philosophical Magazine Letters* 96 (2016) 416–424.

[14] S.A. Mantri, D. Choudhuri, T. Alam, G.B. Viswanathan, J.M. Sosa, H.L. Fraser, R. Banerjee, *Scripta Materialia* 154 (2018) 139–144.

[15] S.A. Mantri, D. Choudhuri, A. Behera, J.D. Cotton, N. Kumar, R. Banerjee, *Metall and Mat Trans A* 46 (2015) 2803–2808.

[16] R. Dong, J. Li, H. Kou, J. Fan, Y. Zhao, H. Hou, L. Wu, *Journal of Materials Science & Technology* 44 (2020) 24–30.

[17] B. Song, W. Xiao, C. Ma, L. Zhou, *Materials Characterization* 148 (2019) 224–232.

[18] Y. Zheng, R.E.A. Williams, J.M. Sosa, T. Alam, Y. Wang, R. Banerjee, H.L. Fraser, *Acta Materialia* 103 (2016) 165–173.

[19] Y. Zheng, R.E.A. Williams, D. Wang, R. Shi, S. Nag, P. Kami, J.M. Sosa, R. Banerjee, Y. Wang, H.L. Fraser, *Acta Materialia* 103 (2016) 850–858.

[20] S. Nag, Y. Zheng, R.E.A. Williams, A. Devaraj, A. Boyne, Y. Wang, P.C. Collins, G.B. Viswanathan, J.S. Tiley, B.C. Muddle, R. Banerjee, H.L. Fraser, *Acta Materialia* 60 (2012) 6247–6256.

[21] Y. Ni, A.G. Khachaturyan, *Nature Mater* 8 (2009) 410–414.

[22] A. Boyne, D. Wang, R.P. Shi, Y. Zheng, A. Behera, S. Nag, J.S. Tiley, H.L. Fraser, R. Banerjee, Y. Wang, *Acta Materialia* 64 (2014) 188–197.

[23] J.M. Sosa, D.E. Huber, B. Welk, H.L. Fraser, *Integrating Materials* 3 (2014) 123–140.

[24] D. Choudhuri, Y. Zheng, T. Alam, R. Shi, M. Hendrickson, S. Banerjee, Y. Wang, S.G. Srinivasan, H. Fraser, R. Banerjee, *Acta Materialia* 130 (2017) 215–228.

[25] L.T. Stephenson, M.P. Moody, P.V. Liddicoat, S.P. Ringer, *Microsc Microanal* 13 (2007) 448–463.

[26] J.M. Hyde, E.A. Marquis, K.B. Wilford, T.J. Williams, *Ultramicroscopy* 111 (2011) 440–447.

[27] H.P. Ng, A. Devaraj, S. Nag, C.J. Bettles, M. Gibson, H.L. Fraser, B.C. Muddle, R. Banerjee, *Acta Materialia* 59 (2011) 2981–2991.

[28] M. Sluiter, P.E.A. Turchi, *Phys. Rev. B* 43 (1991) 12251–12266.

[29] F. Findik, *Materials & Design* 42 (2012) 131–146.

[30] W. Fuming, H.M. Flower, *Materials Science and Technology* 5 (1989) 1172–1177.

[31] C. Ghosh, J. Basu, D. Ramachandran, E. Mohandas, *Acta Materialia* 121 (2016) 310–324.

[32] S. Suwarno, J.K. Solberg, J.P. Maehlen, B. Krogh, V.A. Yartys, *Journal of Alloys and Compounds* 582 (2014) 540–546.

[33] T. Zhang, D. Wang, Y. Wang, *Acta Materialia* 196 (2020) 409–417.